Biophysical Chemistry 138 (2008) 42–49

Contents lists available at ScienceDirect

Biophysical Chemistry

journal homepage: http://www.elsevier.com/locate/biophyschem

Molecular dynamics simulations of the bacterial periplasmic heme binding proteins ShuT and PhuT

Ming Liu [a], Ji Guo Su [a,b], Ren Kong [a], Ting Guang Sun [a], Jian Jun Tan [a], Wei Zu Chen [a], Cun Xin Wang [a,*]

[a] College of Life Science and Bioengineering, Beijing University of Technology, Beijing 100124, China
[b] College of Science, Yanshan University, Qinhuangdao 066004, China

ARTICLE INFO

Article history:
Received 29 April 2008
Received in revised form 1 September 2008
Accepted 1 September 2008
Available online 6 September 2008

Keywords:
Protein binding proteins
Heme
PhuT
ShuT
Molecular dynamics simulation
Gaussian network model
Principal component analysis

ABSTRACT

ShuT and PhuT are two periplasmic heme binding proteins that shuttle heme between the outer and inner membranes of the Gram-negative bacteria. Periplasmic binding proteins (PBPs) generally exhibit considerable conformational changes during the ligand binding process, whereas ShuT and PhuT belong to a class of PBPs that do not show such behavior based on their *apo* and *holo* crystal structures. By employing a series of molecular dynamic simulations on the ShuT and the PhuT, the dynamics and functions of the two PBPs were investigated. Through monitoring the distance changes between the two conserved glutamates of ShuT and PhuT, it was found the two PBPs were more flexible than previously assumed, exhibiting obvious opening–closing motions which were more remarkable in the *apo* runs of ShuT. Based on the results of the domain motion analysis, large scale conformational transitions were found in all *apo* runs of ShuT and PhuT, hinting that the domain motions of the two PBPs may be intrinsic. On the basis of the results of the principle component analysis, distinct opening–closing and twisting motion tendencies were observed not only in the *apo*, but also in the *holo* simulations of the two PBPs. The Gaussian network model was applied in order to analyze the hinge bending regions. The most important bending regions of ShuT and PhuT are located around the midpoints of their respective connecting helixes. Finally, the flexibilities and the details of the simulations of ShuT and PhuT were discussed. Characterized by the remarkably large flexibilities, the loop constituted by Ala 169, Gly170 and Gly171 of ShuT and the β-turn constituted by Ala176, Gly177 and Gly178 of PhuT may be important for the functions of the two PBPs. Furthermore, the Asn254 of ShuT and the Arg228 of PhuT may be indispensable for the binding or unbinding of heme, since it is involved in the important hydrogen bonding to the propionate side-chains of heme.

1. Introduction

Located between the inner and outer membrane of the Gram-negative bacteria, periplasmic binding proteins (PBPs) mediate solute transport or initiate chemotaxis by activating flagellar motion [1–3]. Having only one membrane, Gram-positive bacteria employ a similar but membrane-anchored version of PBPs [4,5]. Furthermore, several eukaryotic receptors contain extracellular ligand binding domains that are homologous to PBPs [2]. PBPs bind a great variety of substrates ranging from sugars, amino acids, and peptides to a variety of ion compounds and vitamins [6]. Accordingly, the PBP family consists of many proteins with diverse primary structures. Despite obvious diversity in their primary structures, all PBPs share a very similar tertiary structure, namely: two globular domains connected by a variable connecting domain. Based on the similarities of the primary structure [1,7] or on the topology of their globular domains [8–10], PBPs can be divided into three classes, which are characterized by the number of the connecting domains. Three classes have been identified and classes I, II and III have three, two, and one connecting domains, respectively [3,11].

The connecting domains of the classes I and II PBPs are constituted by either three or two flexible β-strands respectively, whereas the connecting domain of the PBPs of the class III are constituted by a long rigid α-helix. During the substrate binding process, the two lobes of the PBPs belonging to classes I and II twist and get close to each other, and eventually enclose the ligand, resembling a Venus flytrap [2]. Unlike the PBPs of classes I and II, the PBPs of class III do not show significant differences between the ligand-free (*apo*) and the ligand-bound (*holo*) states on the basis of crystal structures [11–18]. As far as these observations are concerned, it is natural to expect that the PBPs of the third class may adopt a different mechanism to capture their substrates. According to a previous study [19], however, it was revealed that the bacterial periplasmic vitamin B_{12} binding protein BtuF which belongs to a class III PBP, is more flexible than previously assumed. The *apo* structure of BtuF fluctuated between the open and the closed states, resembling a Venus flytrap, whereas the *holo* BtuF

* Corresponding author. Tel.: +86 10 67392724; fax: +86 10 67392837.
E-mail address: cxwang@bjut.edu.cn (C.X. Wang).

0301-4622/$ – see front matter © 2008 Elsevier B.V. All rights reserved.
doi:10.1016/j.bpc.2008.09.001

stayed in a stable closed state during molecular dynamics (MD) simulations [19]. The ShuT from Shigella dysenteriae and the PhuT from *Pseudomonas aeruginosa* are two bacterial periplasmic heme binding proteins, which shuttle heme between the outer and the inner membranes [14]. Characterized by their singular connecting α-helixes, the two newly crystallized PBPs obviously fall into the third class. Both the *apo* and *holo* structures of the ShuT were crystallized. The C_α root mean square deviation (RMSD) between the two structures is merely 0.51 Å, and no obvious conformational differences were found between the two structures. For PhuT, only the holo structure was determined, and the C_α RMSD between the holo ShuT and the holo PhuT for 232 common C_α atoms is 1.4Å. By comparing all crystallized PBPs of the third class [11–13,15–18], it was shown that ShuT and PhuT more closely resembled BtuF which reflected the closer similarity in ligands, i.e. heme and B_{12}. Since having a similar tertiary structure with BtuF, it is reasonable to speculate that PhuT and ShuT may share a similar mechanism.

In this current work, a series of MD simulations were applied in order to investigate both the dynamics and the functions of the two periplasmic heme binding proteins. According to the MD trajectories, it was found that both of the two PBPs were capable of exhibiting large scale conformational changes in their *apo* forms to some extent, resembling a Venus flytrap. Particularly, clear opening–closing motions were observed in two of the *apo* ShuT simulations. Based on the domain motion analysis (DMA) and the principal component analysis (PCA), we found the domain motions of the two PBPs were mainly subjected to closure motions. The hinge bending regions of the two PBPs were also given by the results of DMA, and these bending regions were validated by using the Gaussian Network Model. According to these analyses, it was suggested that the residues around the midpoints of the connecting helixes of ShuT and PhuT were important for the opening–closing motions of the two PBPs. Finally, the flexibilities of the two PBPs were discussed according to the details of the MD simulations. Characterized by the large root mean square fluctuations, it was suggested that the β-turn constituted by Ala176, Gly177 and Gly178 in PhuT, and the loop around Ala169, Gly 170, and Gly171 in ShuT may be related to the functions of the two PBPs. In addition to this, we discovered that the hydrogen bond between the propionate side-chains of heme and the Asn254 of ShuT and the Arg228 of PhuT were critical for the stabilization of the two PBPs.

2. Materials and methods

2.1. Molecular dynamics simulation

The coordinates of the ShuT and the PhuT were downloaded from the Protein Data Bank [20], and altogether nine structures were included (2R79, 2R7A and 2RG7). For the ShuT, whose *holo* and *apo* structures were both crystallized, eight structures were available. Among the eight structures, half of them were from the *holo* group (2R7A), and the other half were from the *apo* group (2RG7). Although there were four structures present in the *holo* group, only one structure (chain A) was bonded by heme according to the corresponding electron density map [19]. As to the PhuT, only one *holo* structure was crystallized. Therefore, in order to investigate the dynamics of the *apo* PhuT, one had to remove the ligand from the *holo* PhuT to "create" an artificial "*apo*" structure.

To compare the dynamics and functions of the bacterial periplasmic heme binding proteins, seven initial simulation systems were set up by employing VMD 1.86 [21]. For all simulation systems, the explicit TIP3 water model was applied [22]. Some sodium and chlorine ions were added in order to neutralize the systems by using the *Autoionize* module of VMD 1.86. All MD simulations were performed with the NAMD 2.6 [23] in a 26 nodes HP cluster, and the CHARMM 27 all-atom force field [24,25] was used. For each simulation, all bond lengths were constrained by employing the SHAKE algorithm [26] and the integration time step of 2 fs was used as well. Every system was simulated at a constant temperature of 310 K and a constant pressure of 1 *atm* through the Langevin piston method [27] for 20 ns. The coordinate for each simulation was saved every 5000 steps. The details of these systems are listed in Table 1.

Table 1
The details about the seven MD simulation systems

MD system[a]	Starting structure[b]	Num of atoms	Simulation time (ns)	Description
ShuT_*holo*	2R7A/A	24097	20	heme-bound
ShuT_*apo*_1	2RG7/A	30523	20	heme-free
ShuT_*apo*_2	2RG7/B	30808	20	heme-free
ShuT_*apo*_3	2RG7/C	30946	20	heme-free
PhuT_*holo*	2R79	23772	20	heme-bound
PhuT_*apo*_1	2R79	23040	20	heme-free
PhuT_*apo*_2	2R79	23040	20	heme-free

[a] The suffix *apo* and *holo* here indicate whether heme is included in the specific system. For ShuT, each system is obtained from different crystal structure; for PhuT, all simulation systems are prepared by processing the only crystal structure of the *holo* PhuT, and the only difference between two *apo* PhuT runs is the seed for allocating the initial velocity.
[b] For PhuT, the PDB entry is given; for ShuT, both the PDB entry and the chain used in the specific run are listed.

2.2. Domain motion analysis

To better understand the conformational changes of ShuT and PhuT, the domain motion analysis (DMA) was performed with the DynDom 1.5 [28] and the default parameters were used. DynDom analyzes the conformational changes of a protein in terms of dynamics domains, hinge axes, and hinge bending regions. This program was performed in three consecutive steps, i.e. searching the dynamics domains, determining the interdomain screw axes and finally determining the bending regions. On completion, the dynamics domains, the screw axes and the bending regions will be given according to the previous calculations. Only when the ratio of interdomain to intra-domain displacement is higher than a given value (one was used in this current work), can the calculations about the interdomain screw axes and the bending regions be reasonable.

2.3. Gaussian network model

Gaussian network model (GNM) is a schematic, coarse-grained model which is topology-based and independent of sequence specificity [29]. It describes the three-dimensional structure of protein as an elastic network of C_α atoms connected by identical harmonic springs within a certain cutoff distance. The GNM method has been proved in numerous application studies to be a simple and useful tool for investigating large scale conformational motions, domain motions, and collective dynamics of the biomolecular systems [30–36]. It was also used to find kinetically hot residues and folding cores of proteins [29,34]. In this current study, the GNM analysis was done by using our own codes with a cutoff of 7.0 Å.

2.4. Principal component analysis

Principal Component Analysis (PCA) enables isolation of the essential subspace from the local fluctuations via the calculation of a set of eigenvectors which describe correlated motions of atoms within the MD simulation [37]. To find out the dominant motion over a MD simulation, it is helpful to filter out all other motions by projecting the whole MD trajectory along the direction described by a selected eigenvector. The projections of a trajectory on the eigenvectors of its covariance matrix are called principal components. Through calculating the two extreme projections on the time-averaged structure from the simulation, one can qualitatively understand the moving directions

of each part of the protein. This method has been proved to be an effective tool for investigating the motion tendencies of proteins from MD simulations [37,38]. In this work, the PCA was performed with a module of Gromacs 3.3 [39], and the trajectories were obtained from the previous MD simulations.

3. Results and discussion

3.1. The overall conformational changes

Conformational changes in PhuT and ShuT occurring over the simulations were monitored by C_α RMSDs computed for each run, with respect to their corresponding starting structures. The RMSDs for the holo and the apo simulations described in Table 1 are plotted in Fig. 1A and B, respectively. As illustrated in Fig. 1A, the RMSDs for the *holo* ShuT and PhuT simulations did not change much after reaching their respective equilibriums. The average RMSD for the *holo* run of ShuT from 7 to 20 ns is 2.26±0.25 Å, whilst the *holo* run of PhuT from 5 to 20 ns is 1.81±0.17 Å. Visualizing the final structures of the *holo* ShuT and PhuT, it seems that both of them were very similar with their respective starting structures. As to the three *apo* ShuT and the two *apo* PhuT simulations (Fig. 1B), the RMSDs were much higher, suggesting the heme-free structures were much more flexible than the heme-bound ones. Amongst the three *apo* runs of ShuT, the fluctuations of RMSDs in the ShuT_*apo*_1 run were the most prominent, which may imply large conformational changes. Although the RMSDs for the ShuT_*apo*_2 run was not as fluctuant as those in the ShuT_*apo*_1 run, the raise of RMSDs in the end of this simulation may imply a conformational transition of the ShuT. The RMSDs plot of the ShuT_*apo*_3 run was relatively smooth, except for the medium fluctuations occurring between 9 and 15 ns. For the RMSD plots of the two *apo* PhuT simulations, one is nearly as fluctuant as the ShuT_*apo*_2 run but with smaller amplitude, whereas the other was relatively smooth.

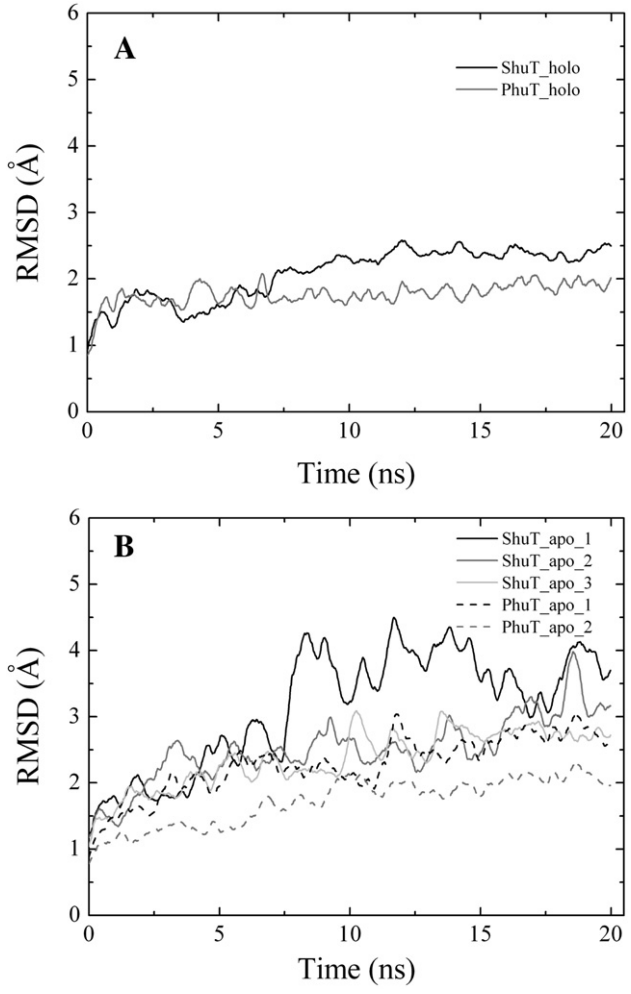

Fig. 1. The C_α RMSDs plots for the *holo* ShuT and PhuT simulations (A), and for the three *apo* ShuT and the two *apo* PhuT simulations (B). All plots in the two figures have been smoothed by the adjacent average method for clarity.

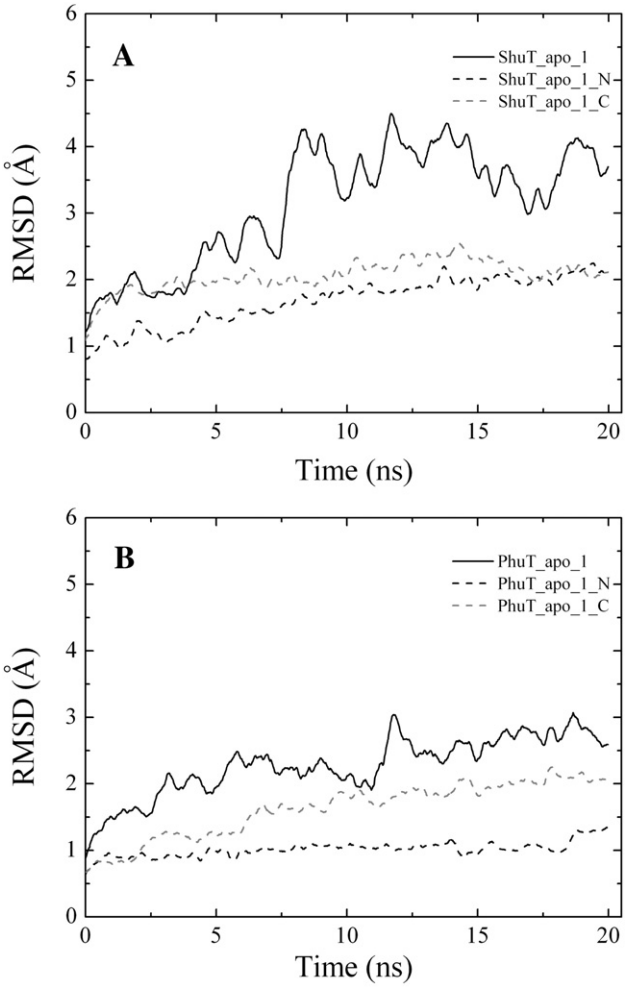

Fig. 2. The C_α RMSDs plots for the ShuT (A) and the PhuT (B) in combination with their respective N- and C-domains. All plots in the two figures have been smoothed by the adjacent average method for clarity.

Suggested by the RMSDs plots for the five independent *apo* runs, it seems that both the ShuT and the PhuT showed conformational changes over their respective simulation processes to some extent. Characterized by large fluctuations of RMSDs, the conformational changes in the ShuT_*apo*_1 and the PhuT_*apo*_1 runs may be the most pronounced in their respective groups. To further investigate these conformational changes, we calculated the RMSDs of the N-domains and the C-domains of the two PBPs for each run, and the results for the ShuT_*apo*_1 and the PhuT_*apo*_1 runs are plotted in Fig. 2A and B, respectively. Fig. 2A shows the RMSDs plots for the N/C-domains of ShuT are very different from those of the overall structure in this very run. The RMSDs for the N- and C-domains are almost much smaller than those of the whole protein over the entire simulation process, excepting for the overlap seen between the C-domain RMSDs plot and the whole protein within the first 5 ns. In Fig. 2B, one can still observe that the RMSDs for the N/C-domains are smaller than those of the whole structure of PhuT in spite of the smaller differences. According

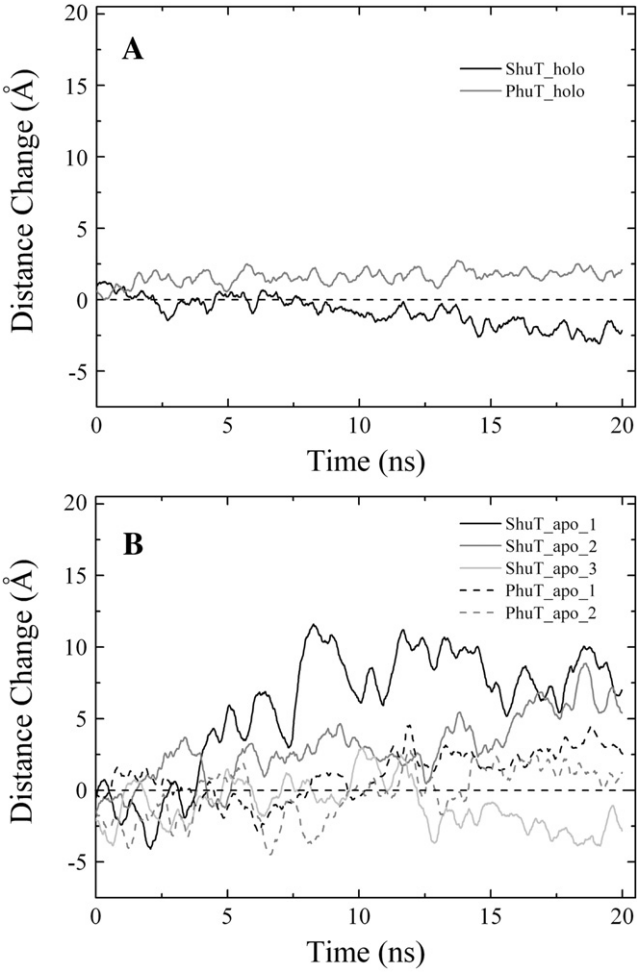

Fig. 3. The distance changes between the C_α atoms of the two glutamate residues in the *holo* ShuT and PhuT simulations (A), and in the three *apo* ShuT as well as the two *apo* PhuT simulations (B). All plots in the two figures have been smoothed by the adjacent average method for clarity.

to these observations, it was indicated that both of the *apo* ShuT and PhuT exhibited relatively large scale conformational changes during simulation processes.

3.2. The domain motions of ShuT and PhuT

From previous studies on BtuF, it has been revealed that two conserved glutamate residues near the apex of each lobe of BtuF acting as negatively charged "knobs" play an important role in the inter-recognition of BtuF and BtuC by inserting into the two positively charged "pockets" on the periplasmic surface of BtuC [40,41]. The distance changes between the C_α atoms of the two conserved glutamate residues, i.e. the Glu50 and Glu180, were calculated as an evaluation of the opening–closing motion of BtuF [19]. Since sharing the similar tertiary structure and topology with BtuF, it is reasonable to monitor the similar property for the two newly crystallized PBPs in order to evaluate the domain motions. By performing a series of BLAST searches [42], it was found that Glu–Glu pair are conserved among the three PBPs (see supplemental figure: SFig. 1), and the Glu78–Glu213 pair of PhuT and the Glu74–Glu207 pair of ShuT might be functionally similar with the Glu50–Glu180 pair of BtuF. The C_α distance changes of the two Glu–Glu pairs are plotted in Fig. 3A and B for the *holo* and *apo* runs, respectively.

As shown in Fig. 3A, owing to the constraint from heme, the Glu–Glu C_α distance changes of the two heme-bound runs fluctuated in a very narrow range from the beginning to the end of the simulations. This result confirms that the *holo* structures of ShuT and PhuT did not exhibit large scale conformational changes during simulation processes, which is basically in line with the observations from the previous B_{12}-bound BtuF simulations [19]. Concerning the five *apo* runs for ShuT and PhuT, the distance change plots displayed much larger fluctuations compared to those of the two *holo* runs. With the distance changes ranging from −5.61 Å to 13.01 Å, the ShuT_*apo*_1 run exhibited a clear opening–closing motion within the 20 ns simulation time scale. The ShuT_*apo*_2 run did not exhibit a clear opening–closing motion within the first 15 ns, however, the Glu–Glu C_α distance in this run increased by 9.3 Å from 5 ns to the end of the simulation compared with the initial conformation. Unlike the first two *apo* runs of ShuT of which the Glu–Glu C_α distance remarkably changed within the 20 ns MD simulations, the C_α distance between the two conserved glutamates in the ShuT_*apo*_3 run did not change that severely. Except for the steep decrease in the distance from 9 ns to 13 ns, this plot was fairly flat compared with those of the first two *apo* runs of ShuT. Moreover, the final structure of ShuT in this run was more compact than the starting structure. With the ranges from −6.46 Å to 3.71 Å and from −6.44 Å to 5.11 Å, the Glu–Glu C_α distance changes for the two *apo* PhuT run were smaller compared with the first two *apo* runs of ShuT, suggesting the domain motions of the *apo* PhuT were not as remarkable as those of the *apo* ShuT. To further explore the domain motions of the two PBPs, the domain motion analysis (DMA) was performed with the DynDom 1.5 [28] and the corresponding results are summarized in Table 2. According to the ratio of interdomain to intradomain displacement, two main conclusions can be drawn. Firstly, all *apo* ShuT and PhuT did exhibit domain motions during MD simulation processes, but the *holo* ones did not. Secondly, the domain motions of *apo* ShuT were more remarkable than those of *apo* PhuT. These findings agree with those obtained directly from the MD trajectories. Furthermore, we also noticed that those domain motions were mainly subjected to the so-called closure type (Table 2) which is synonymous to the opening–closing motions in this very study.

3.3. The bending region analysis

Revealed by previous MD simulations, both of the ShuT and the BtuF [19] are capable of opening and closing in their *apo* forms. By visualizing the trajectories of the ShuT_*apo*_1 simulation, it was found that the maximum distance increase of 13.01 Å (around 8 ns) was accompanied by a bending of the connecting α-helix. The two terminals of this α-helix stretched upwards relative to their respective initial positions, and the linker was bent around its midpoint at which the Asn144 is located (Fig. 4). As to the ShuT_*apo*_2 run, the linker was also bent around the

Table 2
The details about the seven MD simulation systems

MD systems	Min/Max distance change (Å)	Ratio[a]	Domain motion	Closure[b] (%)	Bending residues (Residue number)
ShuT_*holo*	−5.02/2.41	0.77	No	–	–
ShuT_*apo*_1	−5.61/13.01	2.30	Yes	99.1	114–117, 140–144
ShuT_*apo*_2	−3.42/10.23	2.13	Yes	75.6	118–120, 142–143
ShuT_*apo*_3	−6.07/4.36	1.52	Yes	45.1	31–32, 41–44, 116–117
PhuT_*holo*	−0.62/3.85	0.55	No	–	–
PhuT_*apo*_1	−6.46/3.71	1.18	Yes	94.3	145–146, 190–192, 271–272
PhuT_*apo*_2	−6.44/5.11	1.21	Yes	77.5	145–148, 185–192, 225–226, 228–229, 231–232, 235–236, 271–272

[a] The ratio of interdomain to intradomain displacement. In the current work, only when this ration is over one, did we consider that the conformational changes of a protein are caused by domain motions.
[b] The measurement of the degree of closure motion. The higher the value is, the more the domain motion of a protein is like the standard closure motion.

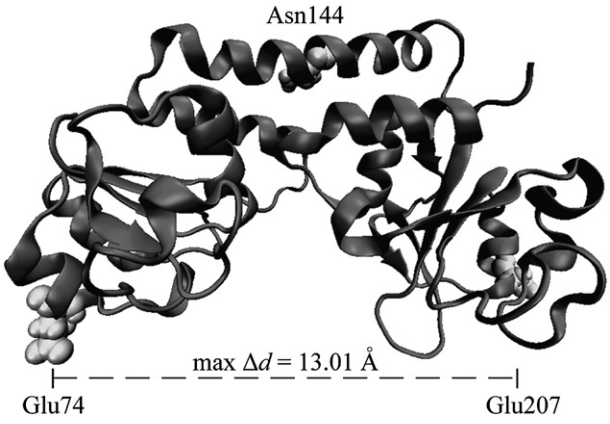

Fig. 4. The extreme conformation of the *apo* ShuT with the largest distance increase of 13.01 Å. The connecting α-helix was obviously bent around the Asn144 which is located at the midpoint of the linker.

Asn144 at 19 ns. These observations reminded us of a similar and even more pronounced phenomenon in the previous MD simulation on BtuF [19]. In that work, a maximum distance increase of 10 Å accompanied by a kink of the connecting α-helix was found. The regular α-helical $n-n+4$ backbone hydrogen bonding pattern was broken around the Ser116 which is also located around the midpoint of the linker [19].

Through performing the DMA, the detailed information about the hinge bending regions of ShuT and PhuT were given in the last column of Table 2. The bending residues of *apo* ShuT can be roughly divided into four regions. Regions I, II, III and IV comprise residues 31 to 32, 41 to 44, 114 to 120, and 140 to144, respectively. As for the PhuT, the bending residues can also be roughly divided into four regions, although the distribution of these bending residues are more scattered than ShuT. Regions I, II, III and IV consist of residues 145 to148, 185 to 192, 225 to 236 and 271 to 272, respectively. Since only two PDB files are needed when performing DMA with DynDom, the data of the bending residues were usually full of much noise. For the sake of validating this data and simplifying the following analyses, the GNM method was performed on the *apo* structures of the two PBPs. The normalized fluctuations driven by the first slowest modes of ShuT and PhuT were plotted in Fig. 5A and B, and the bending regions mentioned above were represented as black dots. Based on our prior knowledge of GNM [33], the bending regions are supposed to be located at the regions where the normalized fluctuations are near to zero. Therefore, only regions III and IV in ShuT, and regions I, and IV were selected for the following analyses. Among these regions, region IV seemed to be indispensable for the domain motions of ShuT, since it could even be detected by visual inspection of the corresponding MD trajectories.

Fig. 6A and B depict the local structures which contain all validated the hinge bending regions for ShuT and PhuT. Fig. 6A shows that the connecting α-helix of ShuT is sandwiched by the two shorter α-helixes which belong to the N- and C-domains, respectively. The two shorter helixes are tightly packed against the two terminals of the center connecting α-helix, thus causing any bending to occur at the two terminals sterically impossible. By contrast, the hindrance around the midpoint of the connecting helix does not seem to be that strong since the shorter helix in the N-domain dips down to the interior of the protein at that very position. Consequently, bending at the midpoint of the connecting helix may be more energetically favorable

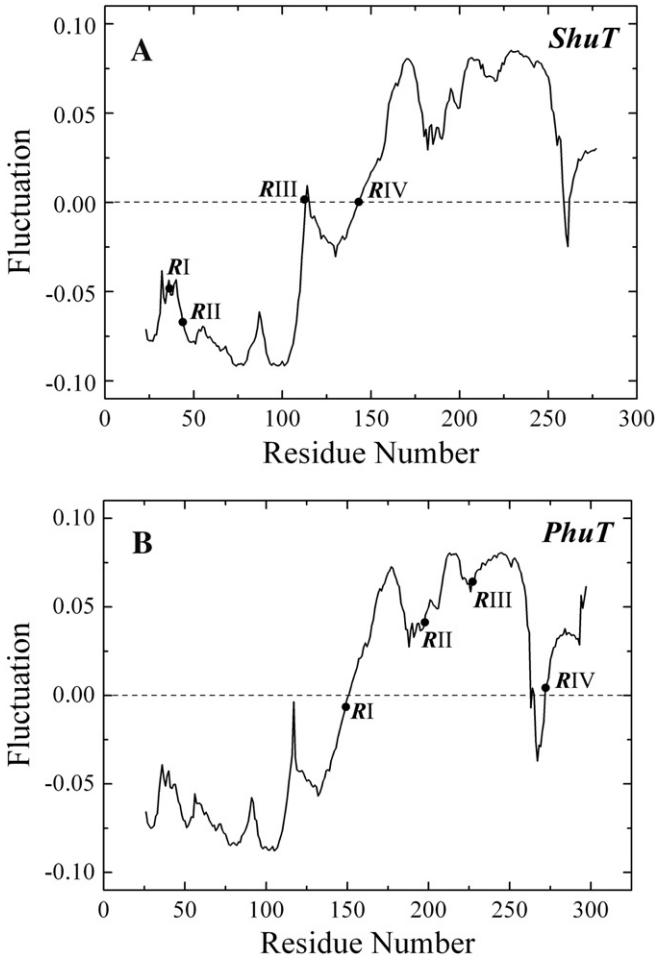

Fig. 5. The normalized fluctuations driven by the slowest modes of ShuT (A) and PhuT (B) calculated by the GNM.

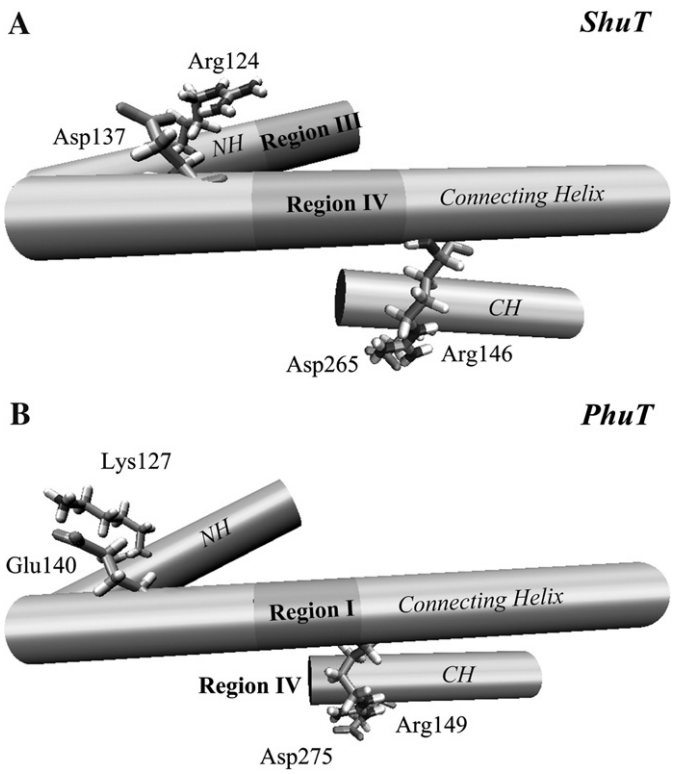

Fig. 6. The local structures of the connecting helix and the two corresponding shorter helixes of ShuT (A) and PhuT (B) are displayed by cartoon representation. The residues involved in the formation of salt bridges are represented by stick model, and the regions that are important for the domain motions are highlighted by the color of dark gray.

Table 3
The first three motion modes of the ShuT and the PhuT in each MD simulation

MD system	Motion modes		
	First	Second	Third
ShuT_*holo*	C[a]/33.5%	N/8.6%	T/6.7%
ShuT_*apo*_1	C/50.1%	T/20.0%	T/7.2%
ShuT_*apo*_2	C/37.1%	T/11.2%	T/9.0%
ShuT_*apo*_3	T[b]/36.0%	C/14.9%	N/6.6%
PhuT_*holo*	N[c]/16.1%	T/11.1%	N/8.9%
PhuT_*apo*_1	T/29.3%	C/13.4%	N/8.9%
PhuT_*apo*_2	C/34.4%	T/11.3%	C/8.1%

[a] Closure motion. In this current study, it is the synonym of opening and closing.
[b] Twisting motion.
[c] Not identified.

than at other positions of the center linker. In addition, this bending region seems to be more important for the opening–closing motion than for the twisting motion, since it is absent from the ShuT_*apo*_3 run (Table 2) whose domain motion was more like a twisting motion. As the counterpart of the region IV of ShuT, the region I in PhuT (Fig. 6B) may play a similar role in the domain motions of PhuT. Although the region III of ShuT was not discovered by visual inspection of the MD trajectories, it did be revealed by the results of DMA on all *apo* runs. Region III is the only reasonable bending region in the ShuT_*apo*_3 run where the closure motion accounts for just 45.1% of the entire domain motions. This suggests that this region is more important for the twisting motion. According to Fig. 6A, the Asp137 and Arg146 in the connecting α-helix make strong electrostatic interactions with the Arg124 and Asp265 in the two shorter helixes, respectively. By applying the Salt Bridge detector of VMD 1.8.6 [21], we found the two shorter helixes were anchored to the connecting helix by forming two salt bridges, thereby highly stabilizing the conformation of the corresponding regions. Based on the previous BLAST analyses (SFig. 1), these four charged residues are conserved between ShuT and PhuT, implying the importance of these residues. Fig. 6A and B shows the region III of ShuT and the region IV of PhuT are located around the salt bridges formed by those conserved residues. Therefore, it seems that these salt bridges may be partly accounted for in the twisting motions of the two PBPs.

3.4. The motion modes of ShuT and PhuT

According to the results of DMA, it was found that the domain motions of ShuT and PhuT were mainly subjected to the closure type. Only in the ShuT_*apo*_3 run, the twisting motion was in the dominant position. To further explore the motion modes of the two PBPs, the PCA method was applied and the dominant motion modes of ShuT and PhuT were revealed. For each simulation, the first three motion modes are listed in Table 3. According to these results, ShuT exhibits not only the opening–closing motion, but also the twisting motion in all MD trajectories. With regard to the PhuT, the twisting motion tendencies were observed both in the *holo* and two *apo* runs, whereas the opening–closing motion tendency was found only in the two *apo* runs. The respective percentages of the first three motion modes to the overall motions are also shown in Table 3. Except for the *holo* PhuT run, the first three motion modes of each run accounted for at least 40% of their respective overall motion. Moreover, the first motion mode of ShuT, i.e. the opening–closing motion, accounted for over 50% of the overall motion, thereby confirming the opening–closing motion is indispensable for the domain motions of ShuT.

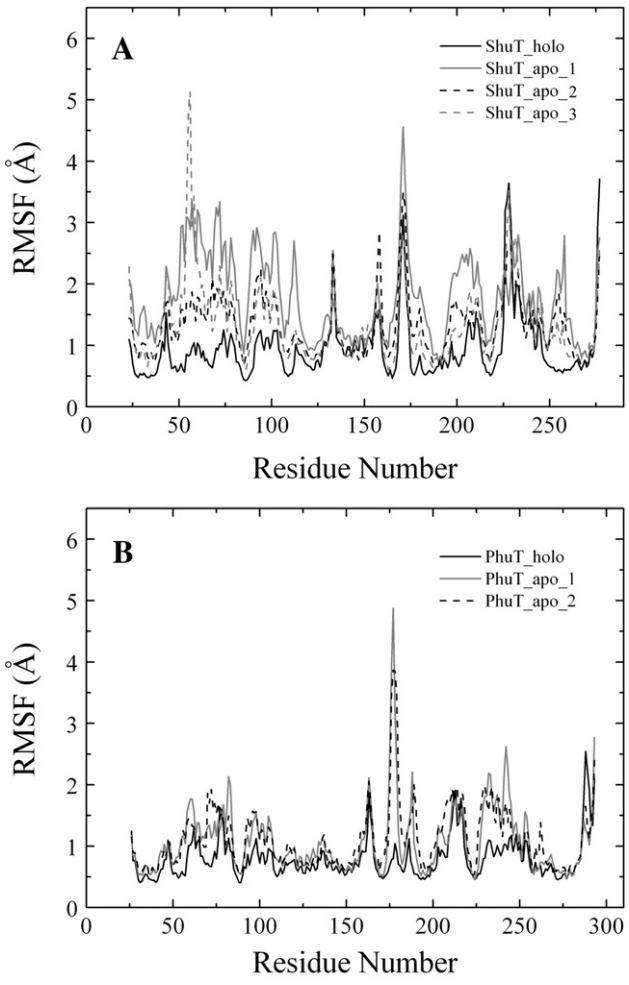

Fig. 8. The C_α RMSFs of the ShuT (A) and PhuT simulations (B) calculated from all of the previous MD simulations.

As a case study, the first three motion modes of the ShuT calculated from the ShuT_*apo*_1 run are depicted by porcupine plots in Fig. 7A, B and C, respectively. The length of the cone in each C_α atom represents the magnitude of movement and the direction is from one extreme conformation to the other. Fig. 7A illustrates the opening–closing

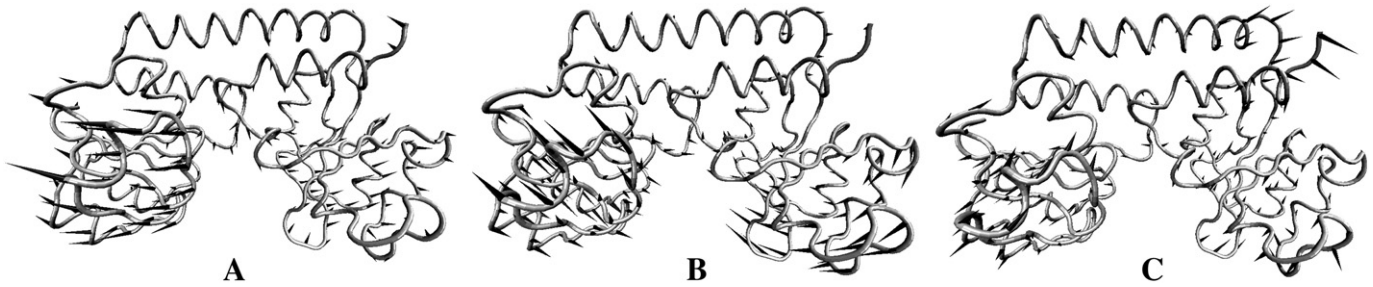

Fig. 7. Porcupine plots of the first (A), second (B) and third motion modes (C) of the *apo* ShuT calculated from the ShuT_*apo*_1 simulation.

motion of ShuT, which has been observed in first two *apo* runs of ShuT. Fig. 7B represents the twisting motion. Despite the small magnitude of movement, the third principle component depicted by Fig. 5C also suggests a twisting-like motion of the ShuT. Combining these results with the observations in the *apo* ShuT simulations, the two lobes of *apo* ShuT not only become close and distant to each other, but they can also twist about the linker as well, all of which are associated with the results obtained from the DMA.

3.5. The flexibilities of PhuT and ShuT

The C_α root mean square fluctuations (RMSFs) of all simulations are calculated as a measurement of the flexibilities of the two PBPs. Fig. 8A and B hold the plots of the RMSFs of both the ShuT and the PhuT simulations, respectively. According to Fig. 8A, it was found that the two lobes (23–131 and 158–277) of ShuT were much more flexible than the connecting α-helix (132–157), especially in the ShuT_*apo*_1 run. This is in accordance with the results of DMA and PCA. The most prominent features in Fig. 9A are the two high peaks around Gly171 and Ile228, which are shared by all of the four ShuT simulations. Gly 171 is located at a loop that connects the two β-strands which are comprised by the residues from 162 to 167 and 175 to 179, respectively. The loop around Gly171 and the nearby short α-helix constituted by the residues ranging form Ile228 to Arg232 were gradually moving close to each other in the *holo* ShuT simulation. Eventually, the carbonyl oxygen of Ala169 in the loop hydrogen, bonded to the guanidinium nitrogen of Arg230 in the short α-helix, thus stabilizing the corresponding local conformation. Although this hydrogen bond was not observed in the three *apo* ShuT simulations, the 169–171 loop and the 228–232 short helix still got close to each other in the three cases. Additionally, the short α-helix constituted by Asp252 to Leu257 seemed to be much more flexible in the three *apo* ShuT runs than in the *holo* ShuT run. When checking the trajectory of the *holo* ShuT simulation, we found that a hydrogen bond formed between the side-chain of Asn254 and the nearby propionate side-chain of heme at the very beginning of the simulation (Fig. 9A). In the *apo* runs, the Asn254 did not hydrogen bond to any substrate any longer; hence facilitating the motion of the corresponding part.

Fig. 8B shows that the most obvious differences among the RMSFs calculated from the three PhuT simulations, emerge from the β-turn constituted by the Ala176, Gly177 and Gly178, which correspond to Ala169, Gly170 and Gly171 of ShuT (SFig. 1), respectively. This β-turn was very flexible in the two *apo* runs of PhuT, but not in the *holo* run. In the two *apo* runs of PhuT, this β-turn pointed towards the five-strand β-sheet of the C-domain at the very beginning, but ended up bending towards the opposite direction, i.e. towards the heme binding pocket. Because of the rearrangement of this β-turn, the conformation of the loop (184–186) connecting with the α-helix (187–196) and the β-strand (179–183) also slightly adjusted during the MD simulation process, thus resulting in large fluctuations in the corresponding positions of PhuT. As for the *holo* run of PhuT, this β-turn was much more stable than in the *apo* runs. By visualizing the MD trajectories of the *holo* PhuT simulation, we found the Arg228 kept hydrogen bonding with the adjacent propionate side-chain of heme (Fig. 9B). Just because of the hydrogen bonding, the motion of the β-turn (176–178) was highly constrained. According to the previous sequence alignment (SFig. 1), it was found the Arg288 of PhuT is corresponding to the Asn222 of ShuT. Although this substitution is conserved, the Asn222 of ShuT is not capable of hydrogen bonding to the propionate side-chains of heme any more. This is due to the binding mode of heme in ShuT is different from that in PhuT. The propionate side-chains of heme pointed to the inside of the heme binding site, rather than in the similar way to the crystal structure of the *holo* PhuT, i.e. to the outside. Owing to the differences in the binding modes of heme, the distance between the propionate side-chains of heme and the Asn222 of ShuT was too large to form hydrogen bonds. It was for this reason that the flexibilities of the 176–178 β-turn of the *holo* PhuT were not comparable to those of the corresponding loop of the *holo* ShuT (Fig. 8A and B). Taking this result into consideration, it was suggested the Arg228 was important for the heme binding process of PhuT.

4. Conclusion

In this study, the dynamics and functions of the two bacterial periplasmic heme binding protein, i.e. PhuT and ShuT, were investigated with MD simulations. Through monitoring the distance changes between the C_α atoms of the two conserved glutamates of ShuT, remarkable opening–closing motions were found in the *apo* ShuT simulations. Furthermore, the connecting α-helix of ShuT were bent at Asn144 which are located around the midpoint of the linker. Based on the results of the DMA, domain motions were found in all *apo* runs of ShuT and PhuT, thus hinting that the domain motions of the two PBPs may be intrinsic. Moreover, distinct opening–closing and twisting motion tendencies were found not only in the heme-free, but also in the heme-bound simulations of ShuT and PhuT on the basis of the results of PCA. Whilst considering these results, it is suggested that

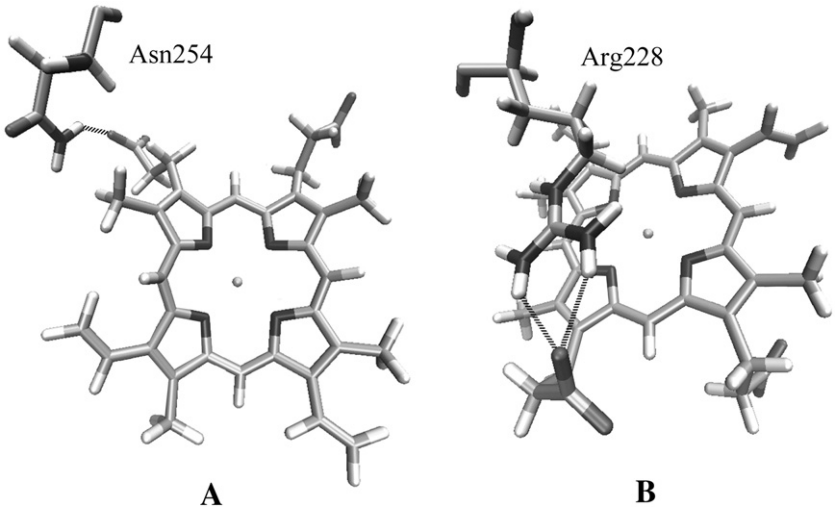

Fig. 9. The two different binding modes of the heme in PhuT (A) and ShuT (B). The Asn254 of ShuT and the Arg228 of PhuT are labeled by corresponding texts and the hydrogen bonds are represented by dashed lines.

ShuT and PhuT may also take the "Venus flytrap" mechanism just as the PBPs of classes I and II do. Combining with the results of GNM analyses, the hinge bending regions of the two PBPs were revealed with the domain motion analysis. The most important bending regions of ShuT and PhuT are located around the midpoints of their respective connecting helixes because of the specific architectures of the two PBPs. This finding is consistent with the visual inspection of the MD trajectories of the *apo* ShuT. Finally, the flexibilities and the details of the simulations of PhuT and ShuT were discussed. Characterized by their remarkably large flexibilities, it was found that the loop constituted by Ala 169, Gly170 and Gly171 of ShuT; and the β-turn constituted by Ala176, Gly177 and Gly178 of PhuT, may be closely related to their respective functions. Furthermore, the Asn254 of ShuT and the Arg228 of PhuT may be indispensable in the binding or unbinding of heme, since they were involved in the important hydrogen bonding to the propionate side-chains of heme.

Acknowledgements

This work was in part supported by grants from the National Natural Science Foundation of China (No. 30670497 and No. 10574009), the Beijing Natural Science Foundation (No. 5072002 and No. 7082006), and the National Basic Research Program of China (No. 2009CB930200).

Appendix A. Supplementary data

Supplementary data associated with this article can be found, in the online version, at doi:10.1016/j.bpc.2008.09.001.

References

[1] R. Tam, M.H. Saier Jr., Structural, functional, and evolutionary relationships among extracellular solute-binding receptors of bacteria, Microbiology and Molecular Biology Reviews 57 (1993) 320–346.
[2] C.B. Felder, R.C. Graul, A.Y. Lee, H.-P. Merkle, W. Sadee, The Venus flytrap of periplasmic binding proteins: an ancient protein module present in multiple drug receptors, AAPS PharmSci 1 (1999).
[3] F.A. Quiocho, P.S. Ledvina, Atomic structure and specificity of bacterial periplasmic receptors for active transport and chemotaxis: variation of common themes, Molecular Microbiology 20 (1996) 17–25.
[4] W. Köster, ABC transporter-mediated uptake of iron, siderophores, heme and vitamin B12, Research in Microbiology 152 (2001) 291–301.
[5] A.J.M. Driessen, B.P. Rosen, W.N. Konings, Diversity of transport mechanisms: common structural principles, Trends in Biochemical Sciences 25 (2000) 397–401.
[6] J.S. Sack, M.A. Saper, F.A. Quiocho, Periplasmic binding protein structure and function. refined X-ray structures of the leucine/isoleucine/valine-binding protein and its complex with leucine, Journal of Molecular Biology 206 (1989) 171–191.
[7] T.E. Clarke, L.W. Tari, H.J. Vogel, Structural biology of bacterial iron uptake systems, Current Topics in Medicinal Chemistry 1 (2001) 7–30.
[8] M.E. Newcomer, G.L. Gilliland, F.A. Quiochol, L-arabinose-binding protein-sugar complex at 2.4 Å resolution. Stereochemistry and evidence for a structural change, Journal of Biological Chemistry 256 (1981) 13213–13217.
[9] J.C. Spurlino, G.Y. Lu, F.A. Quiocho, The 2.3-Å resolution. Structure of the maltose- or maltodextrin-binding protein, a primary receptor of bacterial active transport and chemotaxis, Journal of Biological Chemistry 266 (1991) 5202–5219.
[10] K. Fukami-Kobayashi, Y. Tateno, K. Nishikawa, Domain dislocation: a change of core structure in periplasmic binding proteins in their evolutionary history, Journal of Biological Chemistry 286 (1999) 279–290.
[11] E.L. Borths, K.P. Locher, A.T. Lee, D.C. Rees, The structure of *Escherichia coli* BtuF and binding to its cognate ATP binding cassette transporter, Proceedings of the National Academy of Sciences 99 (2002) 16642–16647.
[12] T.E. Clarke, V. Braun, G. Winkelmann, L.W. Tari, H.J. Vogel, X-ray crystallographic structures of the *Escherichia coli* periplasmic protein FhuD bound to hydroxamate-type siderophores and the antibiotic albomycin, Journal of Biological Chemistry 277 (2002) 13966–13972.
[13] T.E. Clarke, S.Y. Ku, D.R. Dougan, H.J. Vogel, L.W. Tari, The structure of the ferric siderophore binding protein FhuD complexed with gallichrome, Nature Structural & Molecular Biology 7 (2000) 287–291.
[14] W.W. Ho, H. Li, S. Eakanunkul, Y. Tong, A. Wilks, M. Guo, T.L. Poulos, Holo- and Apo-bound structures of bacterial periplasmic heme-binding proteins, Journal of Biological Chemistry 282 (2007) 35796–35802.
[15] N.K. Karpowich, H.H. Huang, P.C. Smith, J.F. Hunt, Crystal structures of the BtuF periplasmic binding protein for vitamin B12 suggest a functionally important reduction in protein mobility upon ligand binding, Journal of Biological Chemistry (2002) M212239200.
[16] M.C. Lawrence, P.A. Pilling, V.C. Epa, A.M. Berry, A.D. Ogunniyi, J.C. Paton, The crystal structure of pneumococcal surface antigen PsaA reveals a metal-binding site and a novel structure for a putative ABC-type binding protein, Structure 6 (1998) 1553–1561.
[17] Y.-H. Lee, R.K. Deka, M.V. Norgard, J.D. Radolf, C.A. Hasemann, Treponema pallidum TroA is a periplasmic zinc-binding protein with a helical backbone, Nature Structural & Molecular Biology 6 (1999) 628–633.
[18] Y.-H. Lee, M.R. Dorwart, K.R.O. Hazlett, R.K. Deka, M.V. Norgard, J.D. Radolf, C.A. Hasemann, The crystal structure of Zn(II)-free *Treponema pallidum* TroA, a periplasmic metal-binding protein, reveals a closed conformation, Journal of Bacteriology 184 (2002) 2300–2304.
[19] C. Kandt, Z. Xu, D.P. Tieleman, Opening and closing motions in the periplasmic vitamin B12 binding protein BtuF, Biochemistry 45 (2006) 13284–13292.
[20] H.M. Berman, J. Westbrook, Z. Feng, G. Gilliland, T.N. Bhat, H. Weissig, I.N. Shindyalov, P.E. Bourne, The protein data bank, Nucleic Acids Research 28 (2000) 235–242.
[21] W. Humphrey, A. Dalke, K. Schulten, VMD: visual molecular dynamics, Journal of Molecular Graphics 14 (1996) 33–38.
[22] W.L. Jorgensen, J. Chandrasekhar, J.D. Madura, R.W. Impey, M.L. Klein, Comparison of simple potential functions for simulating liquid water, Journal of Chemical Physics 79 (1983) 926–935.
[23] L. Kale, R. Skeel, M. Bhandarkar, R. Brunner, A. Gursoy, N. Krawetz, J. Phillips, A. Shinozaki, K. Varadarajan, K. Schulten, NAMD2: greater scalability for parallel molecular dynamics, Journal of Computational Physics 151 (1999) 283–312.
[24] A.D. MacKerell, D. Bashford, M. Bellott, R.L. Dunbrack, J.D. Evanseck, M.J. Field, S. Fischer, J. Gao, H. Guo, S. Ha, D. Joseph-McCarthy, L. Kuchnir, K. Kuczera, F.T.K. Lau, C. Mattos, S. Michnick, T. Ngo, D.T. Nguyen, B. Prodhom, W.E. Reiher, B. Roux, M. Schlenkrich, J.C. Smith, R. Stote, J. Straub, M. Watanabe, J. Wiorkiewicz-Kuczera, D. Yin, M. Karplus, All-atom empirical potential for molecular modeling and dynamics studies of proteins, journal of Physical Chemistry. B 102 (1998) 3586–3616.
[25] A.D.M. Nicolas Foloppe Jr., All-atom empirical force field for nucleic acids: I. Parameter optimization based on small molecule and condensed phase macro-molecular target data, Journal of Computational Chemistry 21 (2000) 86–104.
[26] J.P. Ryckaert, G. Ciccotti, H.J.C. Berendsen, Numerical-integration of Cartesian equations of motion of a system with constraints—molecular- dynamics of *N*-alkanes, Journal of Computational Physics 23 (1977) 327–341.
[27] S.E. Feller, Y. Zhang, R.W. Pastor, B.R. Brooks, Constant pressure molecular dynamics simulation: the Langevin piston method, Journal of Chemical Physics 103 (1995) 4613–4621.
[28] S. Hayward, R.A. Lee, Improvements in the analysis of domain motions in proteins from conformational change: DynDom version 1.50, Journal of Molecular Graphics and Modelling 21 (2002) 181–183.
[29] T. Haliloglu, I. Bahar, B. Erman, Gaussian dynamics of folded proteins, Physical Review Letters 79 (1997) 3090.
[30] S. Kundu, R.L. Jernigan, Molecular mechanism of domain swapping in proteins: an analysis of slower motions, Biophysical Journal 86 (2004) 3846–3854.
[31] I. Bahar, A.R. Atilgan, M.C. Demirel, B. Erman, Vibrational dynamics of folded proteins: significance of slow and fast motions in relation to function and stability, Physical Review Letters 80 (1998) 2733.
[32] L.-W. Yang, I. Bahar, Coupling between catalytic site and collective dynamics: a requirement for mechanochemical activity of enzymes, Structure 13 (2005) 893–904.
[33] J.G. Su, X. Jiao, T.G. Sun, C.H. Li, W.Z. Chen, C.X. Wang, Analysis of domain movements in glutamine- binding protein with simple models, Biophysical Journal 92 (2007) 1326–1335.
[34] Y. Wang, A.J. Rader, I. Bahar, R.L. Jernigan, Global ribosome motions revealed with elastic network model, Journal of Structural Biology 147 (2004) 302–314.
[35] C. Chennubhotla, A.J. Rader, L.-W. Yang, I. Bahar, Elastic network models for understanding biomolecular machinery: from enzymes to supramolecular assemblies, Physical Biology 2 (2005) 5173–5180.
[36] O. Keskin, S.R. Durell, I. Bahar, R.L. Jernigan, D.G. Covell, Relating molecular flexibility to function: a case study of tubulin, Biophysical Journal 83 (2002) 663–680.
[37] A. Amadei, A.B.M. Linssen, D.H.J.C. Berendsen, Essential dynamics of proteins, Proteins, Structure, Function, and Genetics 17 (1993) 412–425.
[38] A. Ivetac, J.D. Campbell, M.S.P. Sansom, Dynamics and function in a bacterial ABC transporter: simulation studies of the BtuCDF system and its components, Biochemistry 46 (2007) 2767–2778.
[39] H.J.C. Berendsen, D. vanderSpoel, R. vanDrunen, Gromacs: a message- passing parallel molecular- dynamics implementation, Computer Physics Communications 91 (1995) 43–56.
[40] R.N. Hvorup, B.A. Goetz, M. Niederer, K. Hollenstein, E. Perozo, K.P. Locher, Asymmetry in the structure of the ABC transporter- ninding protein complex BtuCD- BtuF, Science 317 (2007) 1387–1390.
[41] E.L. Borths, B. Poolman, R.N. Hvorup, K.P. Locher, D.C. Rees, In vitro functional characterization of BtuCD- F, the *Escherichia coli* ABC transporter for vitamin B12 uptake, Biochemistry 44 (2005) 16301–16309.
[42] T.A. Tatusova, T.L. Madden, BLAST 2 S, a new tool for comparing protein and nucleotide sequences, FEMS Microbiology Letters 174 (1999) 247–250.